DOI: 10.1111/cgf.15010
EUROGRAPHICS 2024 / A. Bermano and E. Kalogerakis
(Guest Editors)

COMPUTER GRAPHICS *forum*
Volume 43 (2024), Number 2

Physically Based Real-Time Rendering of Atmospheres using Mie Theory

S. Schneegans[1], T. Meyran[2], I. Ginkel[2], G. Zachmann[1], and A. Gerndt[1,3]

[1]University of Bremen, Germany
[2]Hanover University of Applied Sciences and Arts, Germany
[3]German Aerospace Center (DLR)

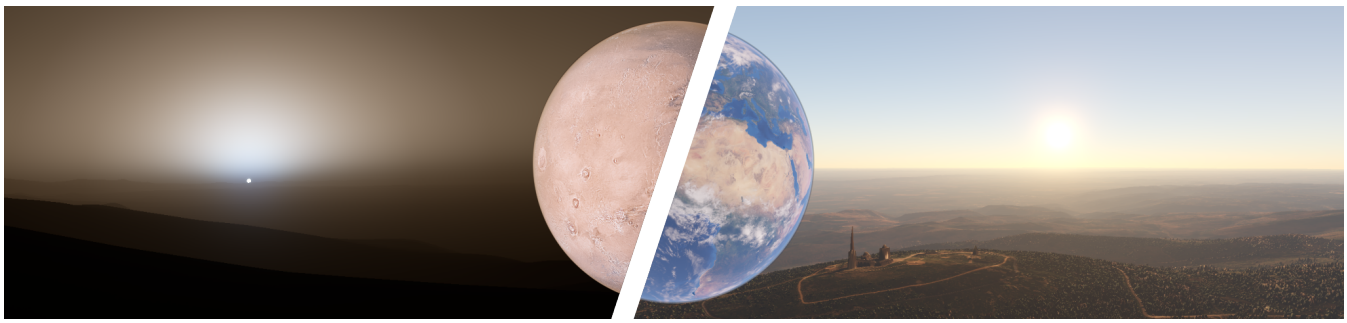

Figure 1: *Our physically-based approach for real-time rendering of atmospheric effects uses Mie Theory for computation of light scattering whereas conventional approaches use approximations which are only valid for Earth's atmosphere. As a result, we can not only visualize Earth's atmosphere but also the thin and dusty atmosphere of Mars which exhibits complex interference effects. As input parameters we use the particle-size distributions, the refractive indices, and the density distributions of the individual constituents of the atmospheres.*

Abstract

Most real-time rendering models for atmospheric effects have been designed and optimized for Earth's atmosphere. Some authors have proposed approaches for rendering other atmospheres, but these methods still use approximations that are only valid on Earth. For instance, the iconic blue glow of Martian sunsets can not be represented properly as the complex interference effects of light scattered at dust particles can not be captured by these approximations. In this paper, we present an approach for generalizing an existing model to make it capable of rendering extraterrestrial atmospheres. This is done by replacing the approximations with a physical model based on Mie Theory. We use the particle-size distribution, the particle-density distribution as well as the wavelength-dependent refractive index of atmospheric particles as input. To demonstrate the feasibility of this idea, we extend the model by Bruneton et al. [BN08] and implement it into CosmoScout VR, an open-source visualization of our Solar System. In a first step, we use Mie Theory to precompute the scattering behaviour of a particle mixture. Then, multi-scattering is simulated, and finally the precomputation results are used for real-time rendering. We demonstrate that this not only improves the visualization of the Martian atmosphere, but also creates more realistic results for our own atmosphere.

CCS Concepts

• ***Computing methodologies*** → *Real-time simulation;*

1. Introduction

The intricate colours of the sky have been awe-inspiring for humans since the dawn of time. For centuries, artists have tried to capture the beauty of the sky in their paintings and scientists have tried to understand the underlying physical processes. When the first images of Martian sunsets were captured by the Viking landers in 1976, the colours of the Martian sky were a surprise to many. Instead of a familiar blue colour, the Martian sky appeared in a muted brown and the sunsets had a blueish tint (see *Figure 2*).

The physical processes which cause the colours of Earth's sky are complex yet well understood and can be sufficiently approximated with simple mathematical models. For instance, the

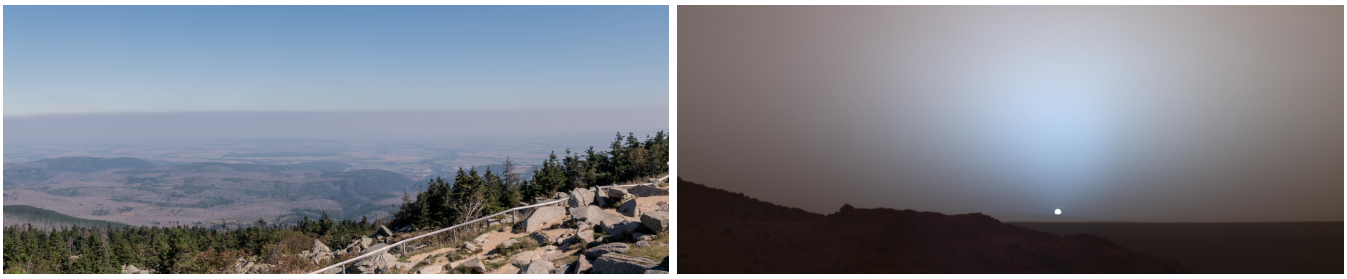

Figure 2: *The sky on Mars looks different from the sky on Earth. The left image shows a view from mount Brocken in Germany photographed by the author. For* Figure 7 *we replicated this scene using the technique described in this paper. The right image shows a sunset on Mars captured by the Spirit Rover in Gusev Crater on Mars. The colour of Earth's sky is predominantly caused by scattering at small air molecules while the colour of the Martian sky is primarily caused by scattering at larger dust particles with a complex refractive index.*

Rayleigh scattering equations can be used to compute light scattering at air molecules causing a blue sky and orange or red sunsets on Earth. Simple parametric functions such as the Henyey-Greenstein phase function can be employed to compute light scattering at aerosols leading to haze and a subtle white halo around the Sun. For several decades, such approximations have been used to simulate the appearance of Earth's sky using computer programs.

While the colours of the Martian sky are caused by the same physical principles, some approximations used for Earth's atmosphere are not applicable to the Martian atmosphere. This is mainly due to the fact that the Martian atmosphere contains a significant amount of dust particles which are approximately the same size as the wavelength of visible light. This causes complex interference effects which can not be captured with the simple parametric functions commonly used in atmospheric rendering models.

However, physically-based visualizations of extraterrestrial skies have a wide variety of applications in the fields of science, education, and entertainment. Planetary researchers could use such simulations to predict the composition of an atmosphere or to plan observations under realistic lighting conditions on distant planets. Interactive visualizations could provide students and the public with engaging tools to explore the intricacies of our Solar System. Such immersive learning experiences could spark interest in space sciences and foster a deeper appreciation for our place in the Cosmos. Video games could transport players to more realistic otherworldly places, or it could be used to enhance the visual effects in movies and television shows, creating more correct and believable scenes.

In this paper, we show that replacing the commonly used approximations with Mie Theory not only improves the rendering of our own atmosphere but also produces better results for the Martian atmosphere. To demonstrate this, we compare our results with the state-of-the-art in real-time rendering of the Martian atmosphere.

2. Physical Background and Related Work

First, we summarize mathematical models for the complex interactions between light and atmospheric particles. While this summary should be sufficient to follow the remainder of the paper, much more information can be found in related text books [Hul57,BH08]. Then, we will show how these models have been used to simulate the appearance of the atmosphere of Earth and Mars.

When light travels through an atmosphere, it is scattered or absorbed by small particles and hence attenuated before it reaches an observer. The amount of scattering and absorption by a given particle is measured with its cross-sections C_{sca} and C_{abs} respectively. Their unit is m^2, and they define the effective "target area" which incident light can "hit". When added, they define the amount of light extinction by an individual particle: $C_{ext} = C_{sca} + C_{abs}$. For a given volume V containing N independent particles, the scattering, absorption, and extinction coefficients β_{sca}, β_{abs}, and $\beta_{ext} = \beta_{sca} + \beta_{abs}$ with the unit m^{-1} are defined as:

$$\beta_{sca} = \frac{\sum_{i=1}^{N} C_{i,sca}}{V} \quad \beta_{abs} = \frac{\sum_{i=1}^{N} C_{i,abs}}{V} \quad \beta_{ext} = \frac{\sum_{i=1}^{N} C_{i,ext}}{V} \quad (1)$$

The independence of the individual particles is very important as it allows deriving the scattering behaviour of a collection of particles by studying a single particle. As described by van de Hulst, inhomogeneities in air (even water drops during dense fog) are sufficiently spaced to ensure independent scattering [Hul57, p. 4f]. These coefficients can be used to compute the attenuated irradiance I when light traveled a distance l through a medium by applying Beer's Law: $I(l) = I_0 e^{-\beta_{ext} l}$.

Besides these extinction coefficients, the phase function $P(\theta, \varphi)$ is required to model a scattering event. It yields the probability of light being scattered into a specific direction (θ, φ). The phase function is defined so that the integral over all directions is one.

2.1. Mie Theory

In 1908, Gustav Mie published a set of equations which can be used to compute the phase function and the extinction cross-sections for spherical particles. He applied Maxwell's equations to fully compute the electromagnetic field caused by light interacting with a homogenous spherical particle [Mie08]. For spherical particles, the phase function does not require two but only one scattering angle θ thanks to the rotational symmetry of spheres. The only other input parameters are the particle's complex refractive index n, and the so-called "size parameter" $x = 2\pi r \lambda^{-1}$ which relates the particle radius r to the wavelength of the incident light λ. The imaginary part of n describes the amount of light which is absorbed by the material. For *Figure 3*, these equations were used to compute the phase function of a small drop of water and the phase function of a mixture of water drops of various sizes.

2.2. Approximations of Mie Theory

The equations developed by Gustav Mie can not be expressed in closed analytical form since they contain an infinite series of Legendre polynomials and spherical Bessel functions. However, if $n-1$ or x converge to zero or infinity, the complex Mie equations can be replaced by approximations, which are usually used in the field of computer graphics.

Very Small Particles: Rayleigh Scattering

In 1871, John William Strutt (also known as Lord Rayleigh) published formulas which can be used to compute the phase function and amount of light scattered by particles which are small when compared to the incident wavelength [Str71]. In this case, the particles start to oscillate with the frequency of the incident light which causes light to be emitted at the same wavelength in nearly all directions in equal amounts and also approximately in phase. Thus, it does not give rise to complex interference patterns. As gas particles are not spherical in practice, a so-called depolarization factor δ is often used [Buc95]. Here, n is the real refractive index of the gas and N the number of molecules per unit volume:

$$P_{gas}(\theta) = \frac{3}{16\pi}\frac{1+3\gamma+(1-\gamma)\cos^2\theta}{1+2\gamma} \quad \text{with} \quad \gamma = \frac{\delta}{2-\delta} \tag{2}$$

$$C_{sca_{gas}} = \frac{24\pi^3}{N^2\lambda^4}\left(\frac{n^2-1}{n^2+2}\right)^2\frac{6+3\delta}{6-7\delta} \tag{3}$$

The intensity of the scattered light is proportional to $\frac{1}{\lambda^4}$. This means that smaller wavelengths are scattered much more effectively than longer wavelengths, which is the primary reason for the blue sky and red sunsets on Earth.

These equations can be used for a non-absorbing medium and for wavelengths which are much larger than the size of the individual molecules. As such, they are suitable for computing the scattering behaviour of molecules in the visible spectrum. However, they can not be used for dust particles of the Martian atmosphere.

Large and Optically Soft Particles: Anomalous Diffraction

H. C. van de Hulst proposed an approach for computing the amount of forward-scattering by large and optically soft ($n \approx 1$) spheres [Hul57, p. 179]. Since the particle's index of refraction is required to be close to one, the light will only marginally deviate from a straight path. However, as the particle is large, there will be a significant phase difference between light which travelled through the particle and light diffracted around the particle. The resulting interference effects are modelled by this approximation.

Costa et al. used this approximation to compute the extinction of light passing through a dust particle in the Martian atmosphere [CBE*21]. This approach may seem questionable at first as most of the particles are relatively small and have a relatively large refractive index of around 1.5 [ECM14]. Thus, we compared their results for C_{ext} with the values from Mie Theory, and the results are indeed very similar at least for dust particles with a radius of more than 0.1 µm. However, we will see that the Martian dust contains a significant amount of smaller particles as well.

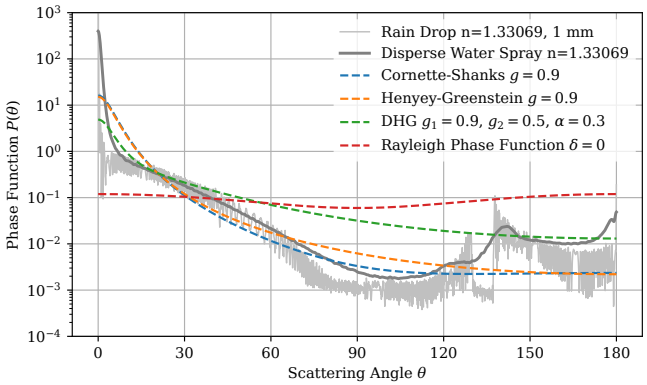

Figure 3: *A phase function describes how likely light is scattered into a given direction during a scattering event. The complex grey line shows the phase function of a rain drop when lit by depolarized red light (650 nm). The valley between 130° and 140° separates the primary rainbow on its right from the secondary rainbow on its left. The numerous wiggles in this curve are caused by the complex interference pattern of the scattered wave. The wiggles are smoothed when not a single particle but a mixture containing a wide variety of particle sizes is simulated (dark grey line). In computer graphics, these functions are often approximated with parametric phase functions, some of which are also shown in this graph.*

Large Particles: Parametric Phase Functions

A fundamentally different approach in modelling light scattering in an atmosphere is to use phase functions and extinction coefficients fitted to measurements. In 1941, L. Henyey and J. Greenstein published a phase function with just one parameter g controlling the amount of forward scattering [HG41].

$$P_{HG}(\theta, g) = \frac{1}{4\pi}\frac{1-g^2}{(1+g^2-2g\cos\theta)^{\frac{3}{2}}} \tag{4}$$

The major drawback of this one-parameter Henyey-Greenstein Phase Function is the lack of a backward-scattering lobe which would be required to capture effects such as glories. To enable this, a three-parameter variant has been proposed [Kat75]. It features a forward-scattering lobe as well as a back-scattering lobe (controlled with the g_1 and g_2 parameters respectively). The symmetry between the two is controlled with the α parameter.

$$P_{DHG}(\theta, g_1, g_2, \alpha) = \alpha P_{HG}(\theta, g_1) + (1-\alpha)P_{HG}(\theta, -g_2) \tag{5}$$

This three-parameter Henyey-Greenstein phase function is said to model Martian dust quite well [CCPHSL19], and it has been used by Costa et al. to perform real-time rendering of the Martian atmosphere [CBE*21]. In *Section 3.2*, we will compare their parametrization with the results from Mie Theory for Martian dust.

Another parametric phase function, which is used frequently in computer graphics, is the "physically reasonable" phase function proposed by Cornette et al. [CS92]. This is controlled by one parameter only, however it features a more intense back-scattering than the standard Henyey-Greenstein phase function. Furthermore, it converges to the Rayleigh phase function for small values of g.

This phase function is used in many approaches for real-time rendering of Earth's atmosphere [NSTN93, BN08, EK10, Hil20].

$$P_{Cornette}(\theta, g) = \frac{3}{2}\frac{1-g^2}{2+g^2}\frac{1+\cos^2\theta}{(1+g^2-2g\cos\theta)^{\frac{3}{2}}} \tag{6}$$

The advantage of using parametric phase functions is that they can be used to approximate the scattering behaviour of a large variety of particles shapes where standard Mie Theory is limited to spherical particles only. On the other hand, the parameters of these phase functions are not directly related to physical properties of the particles and therefore need to be fitted to match measured data. Also, large particles usually exhibit a strong forward-scattering peak which can not be captured by any of the aforementioned parametric phase functions. As we will see, this is especially a problem for Martian dust which features a very pronounced forward scattering. *Figure 3* shows some instances of these commonly used parametric phase functions.

2.3. The Atmosphere of Earth

Air consists of a mixture of gases, such as nitrogen (78 %) and oxygen (21 %) as well as a small amount of aerosols like water droplets or dust particles. The refractive index of the gas mixture varies with wavelength, temperature, and pressure [Pen57]. The distribution of the aerosols is not uniform and depends on the weather conditions.

Earth's Atmosphere in Computer Graphics. A great survey of existing approaches on real-time rendering of Earth's atmosphere has been published by Bruneton et al. in 2016 [Bru16]. In the field of computer graphics, the atmosphere of Earth is traditionally modelled by two constituents: very small air molecules and larger aerosol particles [NSTN93]. Both constituents are modelled with individual phase functions, extinction coefficients, and density distributions. Later approaches also include absorbing gases such as ozone as this has a significant impact on the appearance of the sky especially during sunsets and sunrises [HMS05, Hil20, CBE*21].

For small molecules, Rayleigh scattering is used in nearly all previous works to compute the wavelength-dependent scattering behaviour. The density of the molecules is modelled quite differently; some authors use a set of nested shells of constant density (such as [NSTN93, NDN96, HMS05]), others use a single shell with a hydrostatic density distribution $\rho(h) \propto e^{\frac{h}{H}}$ with H being the scale height [BN08, EK10, Hil20, CBE*21].

To approximate the scattering phase function of larger aerosols, all authors use parametric phase functions. The extinction coefficient $\beta_{ext} = \beta_{sca} + \beta_{abs}$ of aerosols is considered to be independent of wavelength and is usually set to a constant value. An exception is the work by Costa et al. who compute the extinction coefficient β_{ext} using the *Anomalous Diffraction Approximation*, and the scattering coefficient β_{sca} using an approximation based on the atmospheric turbidity [CBE*21]. However, using two unrelated approximations for two related physical properties seems a bit fragile as subtle changes in the parametrization lead to unphysical behaviour such as negative absorption values. Similar to molecules, the density of aerosols is usually modelled with an exponential falloff. However, recent works have emphasized that using more realistic density distributions can significantly improve the results [WVBR*21].

Overall, this modelling of the constituents of an atmosphere can be considered to be the state-of-the art in the field of computer graphics. While newer rendering models such as the widely used Hillaire model can nowadays approximate realistic multiple scattering in real-time without any preprocessing [Hil20], the underlying parametrization and modelling of the constituents has not changed much over the years.

Eric Bruneton concludes his comparison of previous approaches with the statement "[...] that accuracy can still be improved, and that the most promising way to achieve this is to model aerosols more precisely (as opposed to, for instance, simulating more wavelengths, or taking polarization into account)" [Bru16]. Simulating aerosols with Mie Theory seems to be a promising approach to achieve this goal. While Mie Theory has been applied in computer graphics for instance for the simulation of clouds [REK*04] or for the simulation of rainbows [SML*12], it has not been used for a more precise simulation of dust-like aerosols.

2.4. The Atmosphere of Mars

The Martian atmosphere consists primarily of carbon dioxide (95 %) and nitrogen (3 %). It is about eighty times less dense when compared to Earth's atmosphere [ECM14]. Hence, scattering by gas molecules is much less pronounced than on Earth.

Instead, the appearance of the Martian atmosphere is dominated by dust particles. The light scattering behaviour and the distribution of the atmospheric dust on Mars has been studied extensively. Phase functions derived from camera images taken by rovers show an intense forward-scattering peak and a subtle back-scattering lobe [TDL*99, CCPHSL19]. The scattering behaviour has also been studied by analysing orbiter data [WSC*09], and by analysing Martian dust analogue samples in the laboratory [MECM17]. Observations by rovers were used to derive mean particle radii of about $r_{eff} = 1.6\,\mu m$ [TDL*99] or $r_{eff} = 1.5\,\mu m$ [LWS*04]. Additional observations by orbiters and results from models suggest even lower radii especially for dust at higher altitudes [FMR*14, SRM*18, dOA*22]. These radii are approximately in the order of magnitude of the wavelength of visible light giving rise to complex interference patterns.

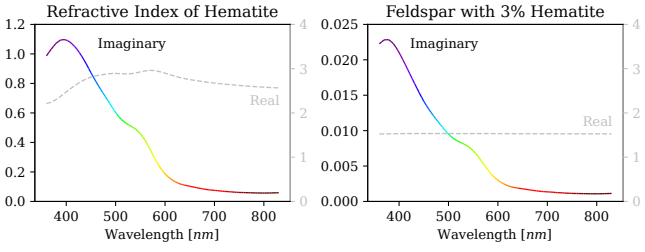

Figure 4: *Hematite has a refractive index which strongly varies with wavelength. The imaginary part shows that it absorbs blue light much more effectively than red light (left graph). According to Ehlers et al., a mixture of feldspar with 3 % hematite is a good approximation for the refractive index of Martian dust (right graph). We followed their work and computed the refractive index of the mixture by applying the Maxwell-Garnett Mixing Rule [ECM14].*

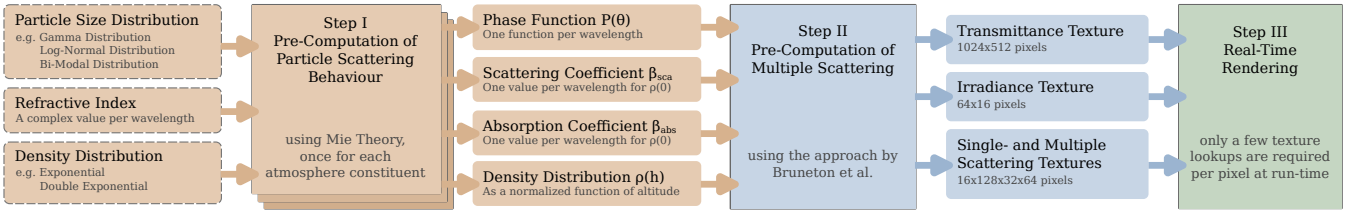

Figure 5: *We use the particle size distribution, the refractive indices of the particles and the particle-density distribution as input. These are used in a first preprocessing step to compute tabulated phase functions, density distributions, and scattering and absorption coefficients for each constituent. Next, multiple scattering is precomputed using the iterative approach by Eric Bruneton [BN08] and stored in lookup textures. During rendering, the precomputed data is used to retrieve the colour of the sky using a few texture lookups only.*

Due to the low gravity and the occasional planet-encircling dust storms, especially small particles can rise up to very high altitudes. The vertical distribution of dust in the atmosphere is complex and varies strongly with location, weather, and season [HRK*11]. However, it can be assumed that the density ρ is roughly proportional to a double-exponential falloff model [Con75]

$$\rho(h) \propto e^{1-e^{\frac{h}{H}}}, \tag{7}$$

where h is the altitude and H is a scale height. This is different from Earth's atmosphere where the density is usually modelled with a single-exponential falloff model.

Dust particles consist primarily of silicates such as feldspar or zeolite containing small percentages of iron oxides such as magnetite (Fe_3O_4) or hematite ($\alpha - Fe_2O_3$) providing the characteristic red colour [CML*01, BSG*16]. Especially fine-grained hematite scatters long wavelengths more effectively than short ones. However, the scattering intensity not only varies with wavelength, but also with the scattering angle. Hematite has a refractive index which causes a strong absorption of blue light (see *Figure 4*). The strong absorption of blue light causes a reduced destructive interference of the blue light transmitted through the particle and blue light diffracted around the particle. Hence, an absorption of blue light actually causes an increase in the amount of blue light scattered into the forward direction. This is one of the reasons which lead to a blue halo around the Sun on Mars [ECM14].

With Mie Theory, we can compute phase functions and extinction coefficients which model this behaviour exactly. It has been shown that even for Martian dust, in which particles are known to be non-spherical, the assumption of spherical particles produces very good results [ECM14]. We will present our simplified model of the Martian dust which simulates all these effects in *Section 3.2*.

The Martian Atmosphere in Computer Graphics. To the best of our knowledge, the only extraterrestrial atmosphere which has been targeted in the research on real-time rendering is in fact the Martian atmosphere. One of the first approaches was published by Collienne et al. [CWGK13]. They used the Bruneton model [BN08] and tweaked its Rayleigh scattering coefficients to visually match photographs taken by Martian rovers. The results show an atmosphere with plausible colours during daytime, however the characteristic blue glow around the Sun during sunrise or sunset is not captured well. Instead, the model by Collienne et al. rather features a bluish glow at the horizon for low Sun elevation angles (see *Figure 10*).

In 2021, Costa et al. presented an alternative approach, also building upon the work of Eric Bruneton [CBE*21]. They incorporated the subtle but existent Rayleigh scattering of molecules in the Martian atmosphere. Furthermore, they replaced the Cornette-Shanks phase function originally used by Eric Bruneton, with a Double Henyey-Greenstein phase function (DHG) following the research by Chen et al. [CCPHSL19]. Chen et al. argued that the DHG fits the scattering behaviour of Martian dust quite well. However, they fitted the DHG parameters to match the sky radiance as observed by the (monochrome) engineering cameras of NASA's Curiosity Rover. The required wavelength-dependent parameters for the DHG were retrieved by "experimental findings" by Costa et al. While this produces more realistic images than the approach by Collienne et al., the resulting images are still quite different when compared to photographs. Especially the strong forward scattering peak of the dust, which causes a small but bright halo around the Sun, is not captured by the DHG. Instead, the model produces a very large and soft glow around the Sun (see *Figure 10*).

3. Atmospheric Rendering using Mie Theory

The key idea of our approach is to precompute the phase function, scattering coefficients, and absorption coefficients using Mie Theory (see *Figure 5*). While the equations of Mie Theory are too complex to be used in real-time rendering, it is possible to evaluate them offline and store the results in lookup tables.

Our atmosphere renderer is implemented into CosmoScout VR [SZGG22], an open source 3D virtual solar system which is based on NASA's SPICE toolkit [Act96]. The source code of CosmoScout VR including the atmosphere renderer and Mie preprocessor is available online [SFG24]. The software allows us to reenact lighting conditions for any given date and location on Earth, Mars, or any other planet or moon. This is important for evaluating the results of our approach.

We chose to base our renderer on the implementation by Eric Bruneton [Bru16]. The primary reason for this decision was to streamline the comparison of our results to previous works regarding the Martian atmosphere. This allows us to compare all three models in a uniform environment. However, it is important to note that our approach of precomputing the scattering behaviour with Mie Theory is not bound to this renderer. Integrating this additional preprocessing step into other systems, such as the newer Hillaire model [Hil20], is a promising task for future works.

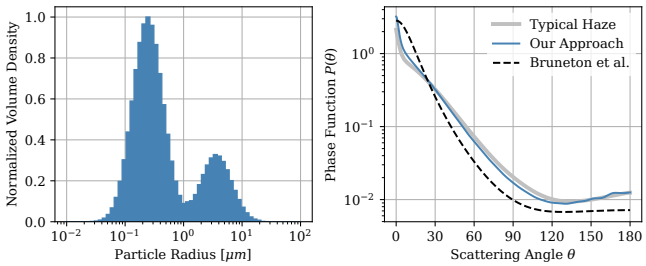

Figure 6: *To simulate haze on Earth, we used the bimodal log-normal size distribution shown on the left ($\mu_1 = -2.5$, $\sigma_1 = 0.6$, $\mu_2 = 0.2$, $\sigma_2 = 0.6$, and a mode ratio of $\gamma = 1000$) and a slightly absorbing refractive index of $n = 1.4 + 0.015i$. The right graph shows the resulting phase function for red light (650 nm). The graph also shows the Cornette-Shanks phase function with $g = 0.76$ used by Bruneton et al. [BN08], as well as a haze phase function retrieved from AERONET data [HES*98].*

Figure 7: *These screenshots show weather conditions generated by different parametrizations of the aerosols. Particles with about 0.1 mm radius and the refractive index of water result in beautiful rainbows. The right image shows a dense layer of haze close to the ground. To simulate this, we used a custom density distribution with a constant density up to an altitude of 700 m followed by a quick exponential falloff. A photograph of a similar situation can be seen in* Figure 2.

3.1. Extending the Bruneton Model

Similar to many other authors, Eric Bruneton models Earth's atmosphere with three constituents: air molecules, aerosol particles, and ozone. Light scattering at air molecules is computed using Rayleigh scattering, aerosols use a wavelength-independent Cornette-Shanks phase function and β_{sca} and β_{abs} for aerosols are computed with Ångström's turbidity formula. Ozone uses measured absorption coefficients. In Bruneton's implementation, the multiple scattering is precomputed iteratively for batches of three wavelengths at a time. The resulting spectral radiance is converted to spectral luminance and accumulated as sRGB values. Finally, the multiple-scattering plus molecule single-scattering and the aerosol single-scattering are stored in two 4D lookup tables.

Our only significant change to Bruneton's 2016 implementation is that the phase functions and density distributions are now sampled from image textures. For each preprocessing batch and at runtime, we upload a floating-point texture containing the phase functions for molecules and aerosols at three wavelengths to the GPU. Similarly, the density distribution is uploaded for the preprocessing as a floating-point texture containing the density values as a function of altitude for all three constituents. Both textures are sampled using linear interpolation. The scattering and absorption coefficients for the current batch of wavelengths are directly injected as constant three-component vectors into the shader code.

Similar to [EK10], we chose to sample the visible spectrum at 15 different wavelengths in order to achieve more realistic results than what would be possible with RGB-only rendering. However, we also follow [BN08, EK10] and defer the evaluation of $P(\theta)$ for molecules and aerosols to the final fragment shader for increased angular precision. For the Martian dust, this function is actually wavelength-dependent, so this part of the algorithm does not act on 15 but only on three wavelengths. However, we found that using multiple wavelengths improved the image quality nonetheless.

To avoid artefacts for the Martian atmosphere, we had to increase the resolution of the precomputed scattering textures. We significantly increased the resolution of the transmittance texture from 256x64 to 1024x512 as this change has a low impact on the preprocessing time but improves rendering of the atmosphere close to the horizon if there are high frequencies in the particle-density distribution. We also increased the original u_v dimension of the scattering texture from 8 to 64 to avoid circular banding around the Sun which occurred for phase functions with an extremely pronounced forward scattering. At the same time, we reduced u_r from 32 to 16 and did not observe any negative effects.

3.2. Precomputing the Particle Scattering Behaviour

As explained above, we introduce an additional preprocessing step which produces tabulated values for $P(\theta)$, β_{sca}, β_{abs}, and $\rho(h)$ for every constituent of the atmosphere. $P(\theta)$, β_{sca}, and β_{abs} can be computed using Mie Theory or by using any of the aforementioned approximations. $\rho(h)$ is sampled at evenly spaced altitudes. The resolution of the resulting lookup tables is configurable, but we found that an angular resolution of $\theta_{steps} = 1024$ for the phase functions is sufficient to represent even the complex phase functions required for rainbows. Also, the particle density is sampled at $h_{steps} = 1024$ different altitudes. The phase functions and the scattering coefficients β_{sca} and β_{abs} are precomputed for a configurable number of wavelengths between 360 nm and 830 nm. For the figures of this paper, we followed [EK10] and used 15 evenly spaced wavelengths. Next, we describe which values were chosen as input for the different atmospheres.

Parametrization of Earth's Atmosphere

In order to visualize the atmosphere of Earth with this generalized model, we need $P(\theta)$, β_{sca}, β_{abs}, and $\rho(h)$ for the three constituents: air molecules, aerosols, and ozone. For ozone, we use the same absorption coefficients and tent-shaped altitude distribution as Bruneton et al. [Bru16]. While it would be possible to use Mie Theory for air molecules, the results would be almost identical to the results from *Equation 2* and *Equation 3*, so we can rather use these much simpler equations during the preprocessing. For *Figure 1* and *Figure 7*, we used the same molecule parameters as [CBE*21]: $\delta = 0.0279$, $N = 2.687\,31 \times 10^{25}\,\mathrm{m}^{-3}$, and n from [Pen57].

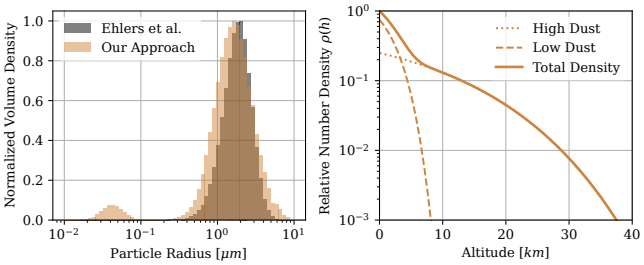

Figure 8: *Left: To simulate Martian dust, we used a bimodal log-normal distribution with the parameters* $r_{eff,small} = 0.04\,\mu m$, $v_{eff,small} = 0.1$, $r_{eff,large} = 1.4\,\mu m$, $v_{eff,large} = 0.35$, *and a mode ratio of* $\gamma = 1000$. *The gamma distribution proposed by Ehlers et al. has a slightly larger effective radius. The consequences on the resulting phase function can be seen in* Figure 9. *Right: We chose a vertical dust distribution composed of more dense low-altitude dust and thinner high-altitude dust (see also* Table 1*).*

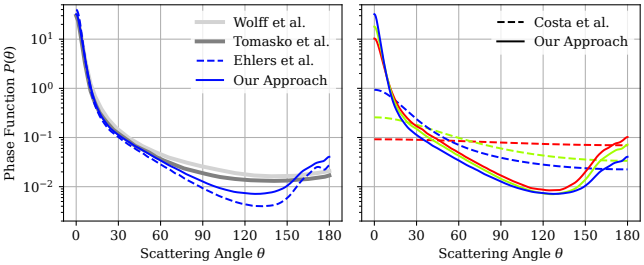

Figure 9: *Left: The simulated Martian dust using a bimodal log-normal distribution scatters light more effectively into directions* $\theta > 90°$ *than the dust simulated by Ehlers et al. The graph also shows phase functions obtained from in-situ measurements on Mars. All phase functions in the left chart are for blue light. Right: Comparison of the phase function of our simulated Martian dust with the DHG phase function used by Costa et al. for red (*680 nm*), green (*550 nm*), and blue (*440 nm*) light (see also* Table 1*).*

However, we can use Mie Theory to simulate a variety of aerosols in Earth's atmosphere. Their vertical distribution and composition varies strongly with location, weather, and season. A significant advantage of our approach is that we can use or mimic measured particle data as input. For Earth's atmosphere, the Aerosol Robotic Network (AERONET) provides such data for many sites on Earth [HES*98]. As a representative example, we use the bimodal log-normal distribution shown in *Figure 6*. The resulting phase function is in very good agreement with AERONET data. It especially features a stronger forward-scattering peak which the Cornette-Shanks phase function is lacking. The density distribution of the aerosols can be specified to recreate various weather conditions. For *Figure 1*, we followed the related work and used an exponentially decreasing density with a scale height of 1200 m. However, using OPAC profiles similar to the work of Wilkie et al. would be possible as well and could further improve the realism [WVBR*21]. With our generalized approach, it would also be possible to simulate other types of particles such as rain, volcanic ash, or smoke. Even if such weather conditions always affect the entire planet in our model, it would be possible to blend between different parametrizations based on the viewer's position or the simulation time. Two example images are shown in *Figure 7*.

Parametrization of the Martian Atmosphere

For scattering at molecules of the Martian atmosphere, we opted for a similar approach to Costa et al., computing the refractive index and molecular number density from the average temperature, pressure, and gas composition of the Martian atmosphere [CBE*21]. The resulting parameters are given in *Table 1*.

For modelling the dust of the Martian atmosphere, we need to specify its refractive index, its particle size distribution, and its density distribution. As described in *Section 2.4*, the refractive index of Martian dust is complex and varies strongly with wavelength. In particular, absorbs blue light which results in an overall reddish appearance. We follow the work of Ehlers et al. and simulate a mixture of feldspar with 3 % hematite [ECM14]. *Figure 4* shows the refractive index of hematite as well as the refractive index of the mixture of feldspar and hematite. In *Section 4*, we will analyse the impact of hematite on the colour of the Martian sky.

For the particle size distribution, Ehlers et al. used a modified gamma distribution. However, there is evidence that Martian dust follows a bimodal log-normal distribution similar to aerosol particles on Earth [FMR*14]. We base our parametrization on the work by Shaposhnikov et al. [SRM*18]. In their work, both the effective radius of the large particles $r_{eff,small}$ and the mode ratio γ depends on the altitude. As we can not model this dependency with our approach, we use the fixed values shown in *Figure 8*. However, these values can be adapted in order to simulate different weather conditions. An exhaustive analysis of the effect of different particle-size distribution on the final appearance of the atmosphere is an interesting task for future works.

As can be seen in *Figure 9*, the resulting phase function is in good agreement with the phase function retrieved from measurements by Tomasko et al. [TDL*99] or Wolff et al. [WTG*10] for scattering angles up to about 90°. For larger angles, the values are lower than the measurements and beyond 150°, there is a strong back-scattering lobe. This over-estimated back-scattering lobe is a well-known issue when approximating the scattering behaviour of non-spherical particles with spherical particles [MTKW97]. It can also be seen that hematite causes red light to be scattered more effectively into all directions except for the forward direction. Here, blue light dominates. Especially in the forward-scattering region, the resulting phase function is much closer to the measurements than the DHG phase function used by Costa et al.

The dust-particle density is the most uncertain parameter. There have been periods of planet-encircling dust storms as well as periods of very low dust density. Hence, the density distribution should be adapted to simulate different weather conditions. For this paper, we chose a vertical dust distribution composed of more dense low-altitude dust and a thinner high-altitude dust (see *Figure 8*). The overall shape of the density profile follows measurements and models [dOA*22]. We added the low-altitude dust component to mimic the conditions seen in the picture captured by the Spirit rover shown in *Figure 2*, which shows a dense layer of dust close to the ground.

		Collienne	Costa	Ours
Molecules	$P(\theta)$	*Equation 2* with $\delta = 0$ [1]	Penndorf Rayleigh: $\frac{0.7629}{4\pi}(1+0.932\cos^2\theta)$ [4]	*Equation 2* with $\delta = 0.09$
	β_{sca}	$[5.75, 13.57, 19.918]\ \mu m^{-1}$ [1]	*Equation 3* with $\delta = 0.09$ and $n = 1.00000337$ [5]	*Equation 3* with $\delta = 0.09$ and $n = 1.00000337$
	$\rho(h)$	$\rho(h) = e^{\frac{-h}{11\,000\,m}}$ [1]	$\rho(h) = e^{\frac{-h}{8000\,m}}$ [4]	$\rho(h) = e^{\frac{-h}{8000\,m}}$
Aerosols	$P(\theta)$	*Equation 6* with $g = 0.76$ [2]	*Equation 5* with $\alpha = 0.743$, $g_1 = [0.67, 0.4, 0.03]$, and $g_2 = 0.094$ [6]	For Mie's equations, we use the IoR from *Fig. 4* and the radius distribution from *Fig. 8*. With $N = 5 \times 10^9\,m^{-3}$, this results in $P(\theta)$ as in *Fig. 9*, $\beta_{sca} = [20.93, 25.39, 30.67]\ \mu m^{-1}$, and $\beta_{abs} = [9.33, 5.25, 1.26]\ \mu m^{-1}$.
	β_{sca}	$3\,\mu m^{-1}$ [3]	$[12.65, 18.51, 23.46]\ \mu m^{-1}$ [7]	
	β_{abs}	$0\,\mu m^{-1}$ [3]	$[24.36, 12.90, 7.852]\ \mu m^{-1}$ [8]	
	$\rho(h)$	$\rho(h) = e^{\frac{-h}{3200\,m}}$ [3]	$\rho(h) = e^{\frac{-h}{11\,100\,m}}$ [4]	$\rho(h) = 0.75 * e^{1-e^{\frac{h}{4000\,m}}} + 0.25 * e^{1-e^{\frac{h}{20\,000\,m}}}$ This function is shown in *Figure 8*.

[1] from [CWGK13] [2] from P. Collienne's source code [3] from [Col13] [4] from [CBE*21] [5] from [CBE*21], however we adapted n to the average surface pressure and temperature on Mars [6] from J. Costa's source code as the values provided in [CBE*21] result in very green sunsets [7] computed using the turbidity-based formula from [CBE*21], however we had to choose a very low turbidity value of $T = 1.01$, else β_{abs} would be negative for the $\kappa = [0.013, 0.006, 0.001]$ from their source code (the κ values from their paper result in a purple atmosphere) [8] computed with $\beta_{abs} = \beta_{ext} - \beta_{sca}$ with β_{ext} from the Anomalous Diffraction Approximation, however we used $N = 2 \times 10^6\,m^{-3}$ from their source code as the value provided in the paper is implausibly large.

Table 1: *This table shows our parametrization as well as the values which we used to reproduce previous works. Wherever three values are given in brackets, they correspond to the wavelengths* $[440\,nm, 550\,nm, 680\,nm]$ *respectively.*

4. Results

Since our approach, the model by Costa et al., and the model by Collienne et al. are all based on the work by Eric Bruneton, we can implement all of them in the same system. Our renderer simply takes a different set of lookup-tables as input.

We believe that our parametrization of the model by Collienne et al. is quite accurate, most likely more accurate than the parametrization by Costa et al., whose images are lacking the intense blue glow at the horizon which should be a key feature of the model by Collienne et al. [CWGK13]. Our implementation of this approach generates images which are very similar to the figures shown in their paper (see *Figure 10*). Reimplementing the model by Costa et al. was more challenging as their paper contains some erroneous numbers. Most notably, the scattering coefficients for molecules are off by at least a factor of 1000, and the index of refraction for CO_2 has not been adapted for the lower pressure and temperature on Mars. Also, the extreme number density of $2.8 \times 10^{35}\ particles/m^3$ for the dust particles is not plausible. We ended up using some parameters from their source code and guessing some others (see *Table 1*). Consequently, our implementation yields some differences when compared to the images presented in the paper by Costa et al. (see *Figure 10*).

The precomputation of the phase functions, density distributions, and scattering coefficients is implemented in C++ using the code published by Bohren et al. [BH08]. The precomputation time scales linearly with the amount of precomputed wavelengths and the number of radius samples used for the particle mixtures. Also, larger particles are slower to compute with Mie Theory. The precomputation typically requires a couple of seconds for our Martian dust model and a couple of minutes for simulating the complex phase functions of a rainbow.

As all the scattering is precomputed, the rendering performance is independent of the type of involved particles. It is very similar to the performance reported by Bruneton et al. as there are no fundamental changes in the rendering logic [BN08]. At run-time, only a few texture lookups are required to retrieve the colour of the sky. Therefore, we will not evaluate the performance in detail in this paper. Furthermore, while our generalized approach features a slightly improved phase function for haze on Earth and can simulate a wide variety of different aerosols, the clear-sky scenario still looks very similar to the renderings by Bruneton et al. Hence, we will rather focus on the evaluation of the Martian atmosphere.

Luminance

First, we compared the luminance of our simulated Martian sky to measured data. Markiewicz et al. measured the radiance of the Martian sky using the Imager for Mars Pathfinder (IMP) camera [MSK*99]. They took a series of images, spanning from the northern horizon over the zenith to the southern horizon. In order to prevent damage to the sensor, they avoided imaging the Sun directly. Judging from the data, the Sun was at an elevation angle of about 75°, and their sampling came as close as about 6° to the Sun.

To replicate this setup, we set the Sun elevation angle to 75°, rendered a full sky dome and sampled this dome with a straight line from the northern horizon over the zenith to the southern horizon, passing the Sun at an angle of 6°. *Figure 11* shows the resulting intensity distribution of our renderer and previous approaches compared to the data from Markiewicz et al. We have normalized the graphs to the same total intensity as we are actually comparing different units here: Markiewicz et al. measured spectral radiance, and we plot the blue-luminance from the tristimulus sRGB space. It can be seen, that our approach reproduces the sharp forward-scattering peak of the Martian dust much better than the previous works.

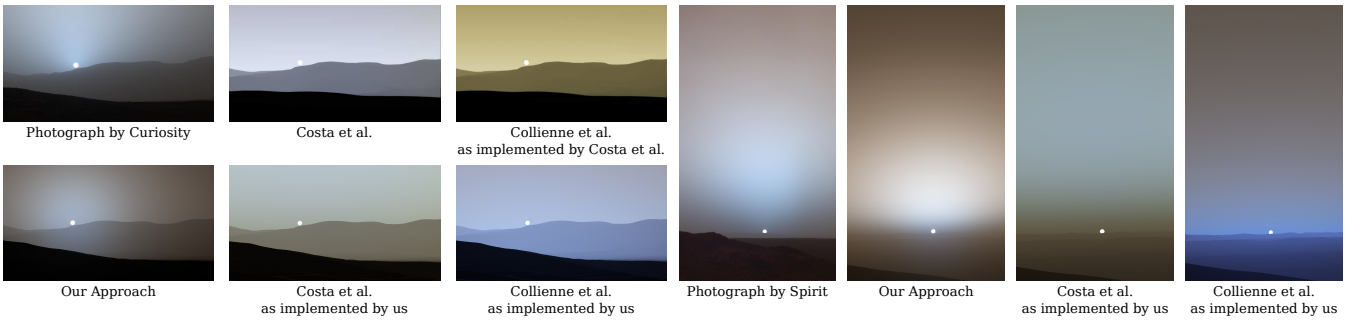

Figure 10: *Comparison for the different rendering approaches to photographs taken by the Martian rovers Curiosity and Spirit. There are significant differences between the approaches and between the implementations. The blue halo around the Sun is very wide in the model of Costa et al. (it is so wide that it is not captured in these images — see* Figure 13 *for a full-sky rendering) and the approach by Collienne et al. rather features a blue glow at the horizon than around the Sun. The two images by Costa et al. are directly taken from their paper [CBE*21].*

Chromaticity

Judging the colour accuracy of a rendering of the Martian sky by looking at photographs is a fragile approach. Usually, a complex processing pipeline is required to turn the raw data into something which corresponds to what a human would perceive on Mars. Also, photographs are often "enhanced" to make the colours more vivid.

Hence, we decided to compare physical chromaticity values of our renderings to measurements. The Mars Exploration Rovers Spirit and Opportunity took chromaticity measurements as part of a sky and horizon survey during their first year on Mars [BISW06]. The data was acquired by the panoramic cameras on top of the rovers. These cameras had been calibrated when they were fitted to the rovers. With this calibration data, it is possible to convert the images to actual physical units. During the campaigns, the cameras captured different portions of the sky and the horizon. The average chromaticity values of these images are shown in *Figure 12*.

For the comparison, the average sky chromaticity values of the presented models were evaluated at Sun elevation angles 0°, 45°, and 90°. On average, the colours produced by all three models are close to the measured data. However, *Figure 13* shows that the colour distribution across the sky varies a lot. While the model by Collienne et al. produces a blue glow only at the horizon, the model by Costa et al. generates more saturated colours and a large blue glow around the Sun which also results in a fair bit of green. Our results are slightly less saturated than the measured data, but this could be due to the fact that the measurements did not include the Sun itself. We averaged the whole sky dome, including the Sun, which adds a bit of blue to the resulting chromaticity values.

With our physically-based model, it is possible to analyse the effect of the physical properties of the dust particles on the appearance of the Martian sky. To demonstrate this, we varied the amount of hematite in the simulated Martian dust. The right chart of *Figure 12* shows that the amount of hematite has a significant impact on the chromaticity values. Without hematite, the Martian sky would be grey and not red. Increasing the amount of hematite beyond 6 % causes the sky to become unrealistically red.

With our approach, blue light dominates in a small region around the Sun (see *Figure 13*). The extent of this blue region seems to vary in reality. There are images available which show nearly no blue light around the Sun and other images which show a very strong blue glow (such as the images shown in *Figure 10*). Different amounts of hematite can not explain this variation. Exploring which physical properties lead to a variation of the extent of the blue glow is an interesting topic for future work.

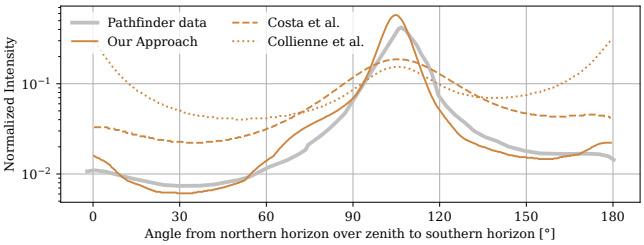

Figure 11: *This graph compares the intensity of the rendered Martian sky to real data. The sharp forward-scattering peak of the simulated Martian dust is in good agreement with the data. The graphs have been normalized to the same total intensity. The Pathfinder data has been retrieved from the 443 nm graph of Figure 1 from [MSK*99]. Missing data points have been interpolated.*

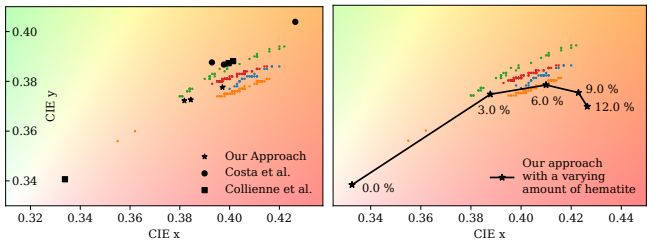

Figure 12: *This graph compares the average chromaticity values of rendered images from* Figure 13 *to real data. The coloured dots represent measurements taken by the Opportunity Sky Survey (green), Opportunity Horizon Survey (red), Spirit Sky Survey (blue), and Spirit Horizon Survey (orange). The amount of hematite in the simulated dust has a significant impact on the chromaticity values.*

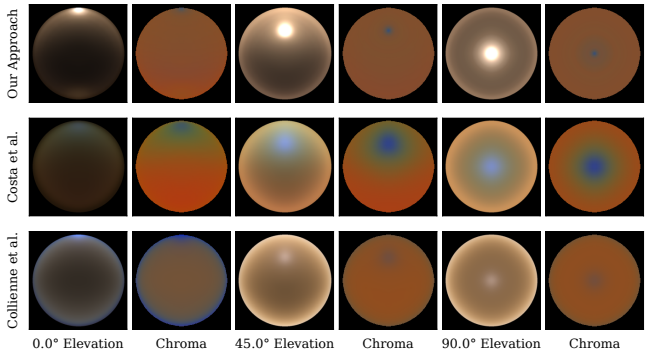

Figure 13: *The images compare our Martian sky to prior approaches. There are differences both in luminance and in chromaticity. For displaying the renderings here, a simple tone-mapping is used: the luminance values of all renderings have been multiplied with a constant (0.00005) and raised to the power of 1/2.2.*

5. Conclusion

In this paper, we have shown that using Mie Theory for precomputing the scattering behaviour of the constituents of an atmosphere is a viable approach for real-time rendering. We based our implementation on the open-source framework by Eric Bruneton [Bru16], however it should be possible to transfer our idea to other atmosphere renderers as well. In our approach, each constituent of an atmosphere is modelled with a wavelength-dependent phase function, wavelength-dependent scattering and absorption coefficients, and a density distribution. These parameters can either be derived from measurements or computed using physical models such as Mie Theory. As we have seen, this enables simulating a wide variety of (global) weather conditions on Earth and Mars. Especially for the latter, conventional parametric phase functions such as the Henyey-Greenstein phase function are not sufficient.

Even if our results are promising and produce images which are in better agreement with measured data than previous works, there is room for improvements. One issue is the over-estimated back-scattering of Martian dust. Results by Wolff et al. suggest that using randomly oriented cylinders may provide a better approximation for Martian dust than using spherical particles [WSC*09]. Analysing more data from Mars and identifying parameters in our model which could explain the observed colours or luminance values is also a promising approach for more realism. With enough data, we could also attempt to visualize the Martian atmosphere directly using measured phase functions and extinction coefficients.

As already shown by Hillaire, the Bruneton model produces artefacts when simulating very thick atmospheres [Hil20]. While this is usually not a problem for Earth and Mars, it may become a problem when we simulate the atmosphere of other planets or moons such as Venus or Titan. Under certain circumstances, we already experienced artefacts when rendering the Martian sky. For instance, the weird shape of the luminance curve in *Figure 11* between 60° and 90° is caused by a circular artefact around the zenith which is only present for certain Sun elevation angles and with relatively thick atmospheres. Using the Hillaire model instead of the Bruneton model could solve this issue but would not be an ideal solution for CosmoScout VR, as this software predominantly renders views from space which the Hillaire model is not really optimized for. Nevertheless, integrating Mie Theory into the Hillaire model is a promising future task and could be of benefit for many applications. It will be interesting to see whether using an isotropic phase function for higher scattering orders is a viable approximation for Martian dust which features a wavelength-dependent and much more pronounced forward-scattering than aerosols on Earth.

For CosmoScout VR, we could also modify the Bruneton model to use path tracing for the primary rays and only use the lookup tables for secondary rays. This would not only reduce artefacts for dense atmospheres, but would also allow for bending of light rays due to refraction, which is simply ignored by most renderers. We will also investigate how we could provide some artistic control, as the extremely pronounced forward-scattering of the Martian dust results in a very high dynamic range of the sky brightness. While this seems to be realistic, it can result in over-exposed renderings.

Overall, the presented approach has significantly enhanced the realism of CosmoScout VR. We often present the virtual solar system to pupils, students, and other visitors. The appearance of the Martian sky is always an inspiring starter for discussions, and we can now confidently say that the Martian sky is rendered with the same physically-based model as the sky of Earth.

Acknowledgements

We thank the reviewers who significantly helped to improve the conciseness of this paper. This work is supported by the German Aerospace Center (DLR) Space Administration with financial means of the German Federal Ministry of Economic Affairs and Climate Action (BMWK) on the basis of a decision by the German Bundestag as part of the VaMEx3-RGE project (50NA2204A). Open Access funding enabled and organized by Projekt DEAL.

References

[Act96] ACTON C. H.: Ancillary data services of NASA's Navigation and Ancillary Information Facility. *Planetary and Space Science 44* (1996), 65 – 70. Planetary data system. 5

[BH08] BOHREN C. F., HUFFMAN D. R.: *Absorption and Scattering of Light by Small Particles*. John Wiley & Sons, 2008. 2, 8

[BISW06] BELL III J. F., SAVRANSKY D., WOLFF M. J.: Chromaticity of the Martian sky as observed by the Mars Exploration Rover Pancam instruments. *Journal of Geophysical Research: Planets 111* (2006). 9

[BN08] BRUNETON E., NEYRET F.: Precomputed atmospheric scattering. In *Computer graphics forum* (2008), vol. 27, Wiley Online Library, pp. 1079–1086. 1, 4, 5, 6, 8

[Bru16] BRUNETON E.: A qualitative and quantitative evaluation of 8 clear sky models. *IEEE transactions on visualization and computer graphics 23* (2016), 2641–2655. 4, 5, 6, 10

[BSG*16] BERGER J. A., SCHMIDT M. E., GELLERT R., CAMPBELL J. L., KING P. L., FLEMMING R. L., MING D. W., CLARK B. C., PRADLER I., VANBOMMEL S. J. V., MINITTI M. E., FAIRÉN A. G., BOYD N. I., THOMPSON L. M., PERRETT G. M., ELLIOTT B. E., DESOUZA E.: A global Mars dust composition refined by the Alpha-Particle X-ray Spectrometer in Gale Crater. *Geophysical Research Letters 43*, 1 (2016), 67–75. 5

[Buc95] BUCHOLTZ A.: Rayleigh-scattering calculations for the terrestrial atmosphere. *Applied Optics 34* (May 1995), 2765–2773. 3

[CBE*21] COSTA J., BOCK A., EMMART C., HANSEN C., YNNERMAN A., SILVA C.: Interactive visualization of atmospheric effects for celestial bodies. *IEEE Transactions on Visualization and Computer Graphics 27* (2021), 785–795. 3, 4, 5, 6, 7, 8, 9

[CCPHSL19] CHEN-CHEN H., PÉREZ-HOYOS S., SÁNCHEZ-LAVEGA A.: Characterisation of Martian dust aerosol phase function from sky radiance measurements by MSL engineering cameras. *Icarus 330* (2019), 16–29. 3, 4, 5

[CML*01] CHRISTENSEN P., MORRIS R., LANE M., BANDFIELD J., MALIN M.: Global mapping of Martian hematite mineral deposits: Remnants of water-driven processes on early Mars. *Journal of Geophysical Research: Planets 106* (2001), 23873–23885. 5

[Col13] COLLIENNE P.: Interactive visualization of parameterized atmospheres in virtual reality, April 2013. Bachelor thesis supervised by Dr. Robin Wolff. 8

[Con75] CONRATH B. J.: Thermal structure of the Martian atmosphere during the dissipation of the dust storm of 1971. *Icarus 24* (1975). 5

[CS92] CORNETTE W. M., SHANKS J. G.: Physically reasonable analytic expression for the single-scattering phase function. *Applied Optics 31* (1992), 3152–3160. 3

[CWGK13] COLLIENNE P., WOLFF R., GERNDT A., KUHLEN T.: Physically based rendering of the Martian atmosphere. In *Workshop der GI-Fachgruppe VR/AR* (2013), Shaker Verlag, Aachen, pp. 97–108. 5, 8

[dOA*22] D'AVERSA E., OLIVA F., ALTIERI F., SINDONI G., CARROZZO F. G., BELLUCCI G., FORGET F., GEMINALE A., MAHIEUX A., AOKI S., ET AL.: Vertical distribution of dust in the Martian atmosphere: OMEGA/MEx limb observations. *Icarus 371* (2022). 4, 7

[ECM14] EHLERS K., CHAKRABARTY R., MOOSMÜLLER H.: Blue moons and Martian sunsets. *Applied Optics 53* (2014). 3, 4, 5, 7

[EK10] ELEK O., KMOCH P.: Real-time spectral scattering in large-scale natural participating media. In *Proceedings of the 26th Spring Conference on Computer Graphics* (2010), pp. 77–84. 4, 6

[FMR*14] FEDOROVA A. A., MONTMESSIN F., RODIN A. V., KORABLEV O. I., MÄÄTTÄNEN A., MALTAGLIATI L., BERTAUX J.-L.: Evidence for a bimodal size distribution for the suspended aerosol particles on Mars. *Icarus 231* (2014), 239–260. 4, 7

[HES*98] HOLBEN B. N., ECK T. F., SLUTSKER I. A., TANRÉ D., BUIS J., SETZER A., VERMOTE E., REAGAN J. A., KAUFMAN Y., NAKAJIMA T., ET AL.: Aeronet—a federated instrument network and data archive for aerosol characterization. *Remote sensing of environment 66* (1998), 1–16. 6, 7

[HG41] HENYEY L., GREENSTEIN J.: Diffuse radiation in the galaxy. *Annales d'Astrophysique 3* (01 1941), 117–137. 3

[Hil20] HILLAIRE S.: A scalable and production ready sky and atmosphere rendering technique. *Computer Graphics Forum 39* (2020), 13–22. 4, 5, 10

[HMS05] HABER J., MAGNOR M., SEIDEL H.-P.: Physically-based simulation of twilight phenomena. *ACM Transactions on Graphics (TOG) 24* (2005), 1353–1373. 4

[HRK*11] HEAVENS N., RICHARDSON M., KLEINBÖHL A., KASS D., MCCLEESE D., ABDOU W., BENSON J., SCHOFIELD J., SHIRLEY J., WOLKENBERG P.: The vertical distribution of dust in the Martian atmosphere during northern spring and summer: Observations by the mars climate sounder and analysis of zonal average vertical dust profiles. *Journal of Geophysical Research: Planets 116* (2011). 5

[Hul57] HULST H. C.: *Light Scattering by Small Particles*. John Wiley & Sons, 1957. 2, 3

[Kat75] KATTAWAR G. W.: A three-parameter analytic phase function for multiple scattering calculations. *Journal of Quantitative Spectroscopy and Radiative Transfer 15* (1975), 839–849. 3

[LWS*04] LEMMON M., WOLFF M., SMITH M., CLANCY R., BANFIELD D., LANDIS G., GHOSH A., SMITH P., SPANOVICH N., WHITNEY B., ET AL.: Atmospheric imaging results from the Mars exploration rovers: Spirit and Opportunity. *Science 306* (2004), 1753–1756. 4

[MECM17] MUÑOZ O., , ECOBAR-CEREZO J., MORENO F.: Light scattering by Martian dust analogues. In *Proceedings of the 6th workshop on Mars Atmosphere Modelling and Observations* (2017). 4

[Mie08] MIE G.: Beiträge zur Optik trüber Medien, speziell kolloidaler Metallösungen. *Annalen der Physik 330* (1908), 377–445. 2

[MSK*99] MARKIEWICZ W., SABLOTNY R., KELLER H., THOMAS N., TITOV D., SMITH P.: Optical properties of the Martian aerosols as derived from Imager for Mars Pathfinder midday sky brightness data. *Journal of Geophysical Research: Planets 104* (1999), 9009–9017. 8, 9

[MTKW97] MISHCHENKO M. I., TRAVIS L. D., KAHN R. A., WEST R. A.: Modeling phase functions for dustlike tropospheric aerosols using a shape mixture of randomly oriented polydisperse spheroids. *Journal of Geophysical Research: Atmospheres 102* (1997), 16831–16847. 7

[NDN96] NISHITA T., DOBASHI Y., NAKAMAE E.: Display of clouds taking into account multiple anisotropic scattering and sky light. In *Proceedings of the 23rd annual conference on Computer graphics and interactive techniques* (1996), pp. 379–386. 4

[NSTN93] NISHITA T., SIRAI T., TADAMURA K., NAKAMAE E.: Display of the Earth taking into account atmospheric scattering. In *Proceedings of the 20th annual conference on Computer graphics and interactive techniques - SIGGRAPH '93* (1993), ACM Press. 4

[Pen57] PENNDORF R.: Tables of the refractive index for standard air and the rayleigh scattering coefficient for the spectral region between 0.2 and 20.0 μ and their application to atmospheric optics. *Josa 47* (1957), 176–182. 4, 6

[REK*04] RILEY K., EBERT D. S., KRAUS M., TESSENDORF J., HANSEN C. D.: Efficient rendering of atmospheric phenomena. *Rendering Techniques 4* (2004), 374–386. 4

[SFG24] SCHNEEGANS S., FLATKEN M., GERNDT A.: CosmoScout VR 1.9.0, Jan. 2024. URL: https://doi.org/10.5281/zenodo.3381953. 5

[SML*12] SADEGHI I., MUNOZ A., LAVEN P., JAROSZ W., SERON F., GUTIERREZ D., JENSEN H. W.: Physically-based simulation of rainbows. *ACM Transactions on Graphics (Presented at SIGGRAPH) 31* (2012), 3:1–3:12. 4

[SRM*18] SHAPOSHNIKOV D. S., RODIN A. V., MEDVEDEV A. S., FEDOROVA A. A., KURODA T., HARTOGH P.: Modeling the hydrological cycle in the atmosphere of Mars: Influence of a bimodal size distribution of aerosol nucleation particles. *Journal of Geophysical Research: Planets 123* (2018), 508–526. 4, 7

[Str71] STRUTT J. W.: XV. On the light from the sky, its polarization and colour. *The London, Edinburgh, and Dublin Philosophical Magazine and Journal of Science 41* (1871), 107–120. 3

[SZGG22] SCHNEEGANS S., ZEUMER M., GILG J., GERNDT A.: CosmoScout VR: A Modular 3D Solar System Based on SPICE. In *2022 IEEE Aerospace Conference (AERO)* (2022), pp. 1–13. 5

[TDL*99] TOMASKO M., DOOSE L., LEMMON M., SMITH P., WEGRYN E.: Properties of dust in the Martian atmosphere from the Imager on Mars Pathfinder. *Journal of Geophysical Research: Planets 104* (1999), 8987–9007. 4, 7

[WSC*09] WOLFF M., SMITH M., CLANCY R., ARVIDSON R., KAHRE M., SEELOS IV F., MURCHIE S., SAVIJÄRVI H.: Wavelength dependence of dust aerosol single scattering albedo as observed by the Compact Reconnaissance Imaging Spectrometer. *Journal of Geophysical Research: Planets 114* (2009). 4, 10

[WTG*10] WOLFF M. J., TODD CLANCY R., GOGUEN J. D., MALIN M. C., CANTOR B. A.: Ultraviolet dust aerosol properties as observed by MARCI. *Icarus 208* (2010), 143–155. 7

[WVBR*21] WILKIE A., VEVODA P., BASHFORD-ROGERS T., HOŠEK L., ISER T., KOLÁŘOVÁ M., RITTIG T., KŘIVÁNEK J.: A fitted radiance and attenuation model for realistic atmospheres. *ACM Transactions on Graphics 40* (2021). 4, 7